Journal of Nuclear Materials 381 (2008) 302–308

Contents lists available at ScienceDirect

Journal of Nuclear Materials

journal homepage: www.elsevier.com/locate/jnucmat

Characterization of the surface charge of oxide particles of PWR primary water circuits from 5 to 320 °C

M. Barale [a,b,1], C. Mansour [a,b], F. Carrette [b], E.M. Pavageau [b], H. Catalette [b], G. Lefèvre [a], M. Fedoroff [a,*], G. Cote [a]

[a] LECA, CNRS, ENSCP, Université Paris 6, 11 Rue Pierre et Marie Curie, 75005 Paris, France
[b] EDF R&D, Site des Renardières, 77818 Moret-sur-Loing, France

ARTICLE INFO

Article history:
Received 4 February 2008
Accepted 1 September 2008

PACS:
82.70.Dd
81.15.Z
68.43.h
28.41.Fr
28.52.Fa

ABSTRACT

The point of zero charge of three typical oxides found as colloids in PWR primary circuits has been measured by mass titration in a large range of temperature: from 5 to 320 °C for magnetite and cobalt ferrite, from 5 to 125 °C for nickel ferrite. Comparisons with zetametry were performed near room temperature. The protonation thermodynamic constants have been calculated. The standard protonation enthalpy at 298 K is −27 ± 5, −31 ± 6 and −32 ± 7 kJ mol^{-1}, for the three oxides respectively. The sign of the surface charge of these colloidal particles in the temperature conditions of the primary circuit indicates that their adhesion onto the materials of the circuit is favored.

1. Introduction

Corrosion of metallic components of water circuits of pressurized water reactors (PWRs) generates colloidal particles. These particles are transported in the circuits, they adsorb dissolved species, they can deposit and accumulate in certain parts of the circuits. Sorption and deposition give rise to several technical drawbacks. In the primary circuit, deposition of solids with radioactive sorbed elements leads to 'hot' spots, which increase the dosimetry of workers during the maintenance operations. Solid deposits disturb also the hydrodynamic and thermal conditions of circuits and can generate local corrosion [1–3]. In order to control and model these effects, predict their evolution during the functioning of reactors, and, finally, minimize them, it is necessary to understand the mechanisms of transport and deposition of particles, together with the mechanism of sorption of dissolved species.

According to the DLVO theory [4], adhesion between two surfaces is controlled by electrostatic and Van der Waals forces. The latter are always attractive, act over short distance and have a small dependency on surface and solution chemistry. Electrostatic forces are connected to the surface charge and depend strongly on the chemical properties of the solids and on the chemistry of the solution. Depending on the relative charge of the surfaces, these forces can be attractive or repulsive. They have a major effect on the deposition behavior of particles towards a surface [5].

According to the surface complexation theory [6], the surface charge of metallic oxides results from sorption or desorption of protons, leading to positive or negative surface sites, and depends on the pH of the solution. Soluble species can adsorb on the solid surface, depending on the ionic charge of these species and on the surface charge. In turn, adsorbed species modify the surface charge and the electrostatic forces between the particles and the walls of the water circuits. Electrostatic interactions depend also on the concentration of ionic species (ionic strength) in the solution, since ions of charge opposite to the surface charge come close to the surface (double layer) and produce a shielding effect of the surface charge. Thus, in order to understand and predict the behavior of colloidal particles in an aqueous solution in term of adhesion to surfaces and sorption behavior towards dissolved species, it is necessary to know their surface charge and establish its relationship with the chemistry of the particles and with the composition of the solution.

There are essentially two ways for evaluating the surface charge. The first one is the measurement of the mobility of the particles under an electrostatic field (zetametry). This method does not give direct access to the surface charge, but measures the ζ-potential, which is the electrostatic potential at the 'shear plane', which is the limit between the counter ions moving with the particle and the counter ions immobile in the solution. A characteristic parameter is the isoelectric point (IEP), which is the pH value corresponding to zero mobility, zero ζ-potential and hence zero surface charge.

* Corresponding author. Tel.: +33 (0) 156813056; fax: +33 (0) 156813059.
E-mail address: michel-fedoroff@enscp.fr (M. Fedoroff).
[1] Present address: AREVA, 1 Rue B. Marcet, BP 181, 71205 Le Creusot Cedex, France.

0022-3115/$ - see front matter © 2008 Elsevier B.V. All rights reserved.
doi:10.1016/j.jnucmat.2008.09.003

The second way of evaluating the surface charge is to use acid–base titrimetric methods. The surface charge is deduced from the quantity of protons sorbed or desorbed by particles as a function of pH. The surface charge is usually calculated from the balance of protons sorbed and desorbed, referred to the surface area. The characteristic parameter is the point of zero charge (PZC), which is the pH value for which the surface charge equals zero, i.e. positive and negative sites have equal concentrations. Ideally, IEP and PZC should coincide. However, this is not always the case, due to adsorbed impurities, presence of initial surface charge prior to titration, or consumption of protons by other reactions such as the dissolution of the solid. When PZC does not coincide with IEP, it has to be considered as a point of zero net proton charge (PZNPC), which is the pH value when the titration curves achieve a zero balance of adsorbed protons.

The main difficulty of the present study results from the necessity to perform these measurements up to temperatures representative of PWR primary circuits, in which they reach 320 °C. Commercial zetameters do not reach temperatures higher than 70 °C. Classical acid–base titration, in which aliquots of acid or base are periodically added to a suspension of the particles, is rather difficult to use at high temperature and pressure. Hence, we have chosen 'mass titration' [7,8], whose principle is to increase progressively the quantity of solid in the suspension. For the highest quantities of solid, pH achieves a plateau, which is the PZC. In fact, it is not always necessary to use many different increasing quantities of solid. If, after preliminary experiments, the right quantity and starting pH are chosen, the plateau is very quickly achieved. This method is therefore simple and can be rather easily used in an autoclave. It was chosen as the main method in this study between 5 and 320 °C.

As a complement to mass titration, zetametry was used in a temperature range close to room temperature, in order to refer the PZC measurements to IEP.

Colloidal species from PWR circuits are difficult to sample. Moreover, after sampling they do not represent the pristine particles. In the present study, we have chosen to work on model particles of the highest purity and with a known chemical composition and structure, so as to be able to understand and model more easily their behavior. Three colloidal species, which are characteristic of primary circuits of PWR [9,10] were chosen: magnetite (Fe_3O_4), nickel ferrite ($NiFe_2O_4$) and cobalt ferrite ($CoFe_2O_4$). In the present investigation, the study of the influence of the composition of the solution was limited to concentrations of a salt (potassium chloride) that do not lead to specific adsorptions.

2. Materials and methods

2.1. Materials and their characterization

Magnetite, cobalt ferrite and nickel ferrite were commercial products. Magnetite of 99.997% purity was purchased from Alfa Aesar, cobalt and nickel ferrites of 98% purity from Nanostructured and Amorphous Materials Inc (Houston, Texas).

Prior to use, these solids were 'washed' in order to remove superficial impurities, until a constant value of the point of zero charge (PZC) was achieved. Magnetite was washed by 0.01 M KOH solutions. Cobalt ferrite is washed by 0.1 M KOH and then by 0.1 M HNO_3. Nickel ferrite is washed by 10^{-4} M HNO_3. This difference in washing procedures results from the nature of superficial impurities. To remove cations, the washing solution has to be acid and by contrast to remove anions, the washing solution has to be alkaline. Finally, solids were washed by high purity water, filtered and dried.

The main characteristics of these solids are summarized in Table 1.

Magnetite, as observed by scanning electron microscope (SEM), is formed of agglomerates of facetted particles of diameters 100–500 nm (Fig. 1(a)). Nickel ferrite and cobalt ferrite are formed of agglomerates of irregularly shaped particles, smaller than those of magnetite (Fig. 1(b)–(c)). The diameter calculated from BET area measurements, assuming a spherical shape, agrees with the diameter observed by SEM for both ferrites, while it is higher in the case of magnetite. This discrepancy for magnetite is explained by adhesion between particles as evidenced by SEM. The coherence lengths determined from X-ray diffraction line widths are close to but smaller than the observed diameters for the three solids, indicating that the particles include several single crystals or crystalline domains.

X-ray diffraction indicates a crystal structure consistent with the expected solid phases. In the case of magnetite and cobalt ferrite, traces of hematite (Fe_2O_3), and Co_3O_4 were detected, respectively.

The Fe(II)/Fe(III) ratio in magnetite, determined by potentiometric titration, using potassium permanganate, indicates that the proportion of magnetite in the solid is higher than 95%. Thermogravimetric analysis under air flow gives the same result.

The composition of ferrites was determined by inductively coupled plasma optical emission spectrometry (ICPOES). The atomic Co/Fe ratio is 0.50 corresponding to the expected one for cobalt ferrite. For nickel ferrite, the atomic Ni/Fe ratio is 0.54, indicating an excess of nickel.

Table 1 gives also the main impurities detected by ICPOES.

2.2. Mass titration

A known weight of solid was introduced into 5 mL of electrolyte (KCl 10^{-2} mol kg^{-1}) and ultrasonically agitated during 10 min. Initial pH is adjusted by addition of hydrochloric acid or sodium hydroxide solutions. The evolution of pH is then followed as the weight of solid is increased. Preparation of suspensions and measurements were performed under nitrogen to avoid the presence of carbon dioxide.

From 5 to 25 °C, the pH was measured by means of a glass electrode and a double junction electrode Ag/AgCl/3 M KCl. From 25 to 125 °C, the pH was measured by means of a glass electrode combined with a solid (gel) electrolyte Ag/AgCl electrode. The solid state of the electrolyte allows working up to 130 °C by limiting evaporation. Between 250 and 320 °C, the pH was determined with an external pressure balanced reference electrode Ag/AgCl/10^{-3} M KCl (EPBRE) and an yttrium stabilized zirconia pH electrode filled with Cu/Cu_2O as internal Ref. [11–13]. Acetic acid/sodium acetate (0.01 mol kg^{-1}/0.01 mol kg^{-1}) and disodium tetraborate

Table 1
Characteristics of magnetite and ferrites used in the present study, with examples of impurities found

	Magnetite	Cobalt ferrite	Nickel ferrite
Specific surface area ($m^2\ g^{-1}$)	1.68 ± 0.02	17 ± 1	60 ± 1
Shape and mean dimensions	Agglomerates 10–50 μm of ≈100–500 nm particles	Agglomerates 10–20 μm of 50–150 nm particles	Agglomerates 0–20 μm of 10–50 nm particles
Diameter according to BET area (nm)	720	67	18
Coherence length (nm)	35	24	11
Impurities (% w)			
Ca	–	0.3	0.1
Na	0.7	0.6	0.5
Mg	–	0.5	–
Co	–	–	0.2

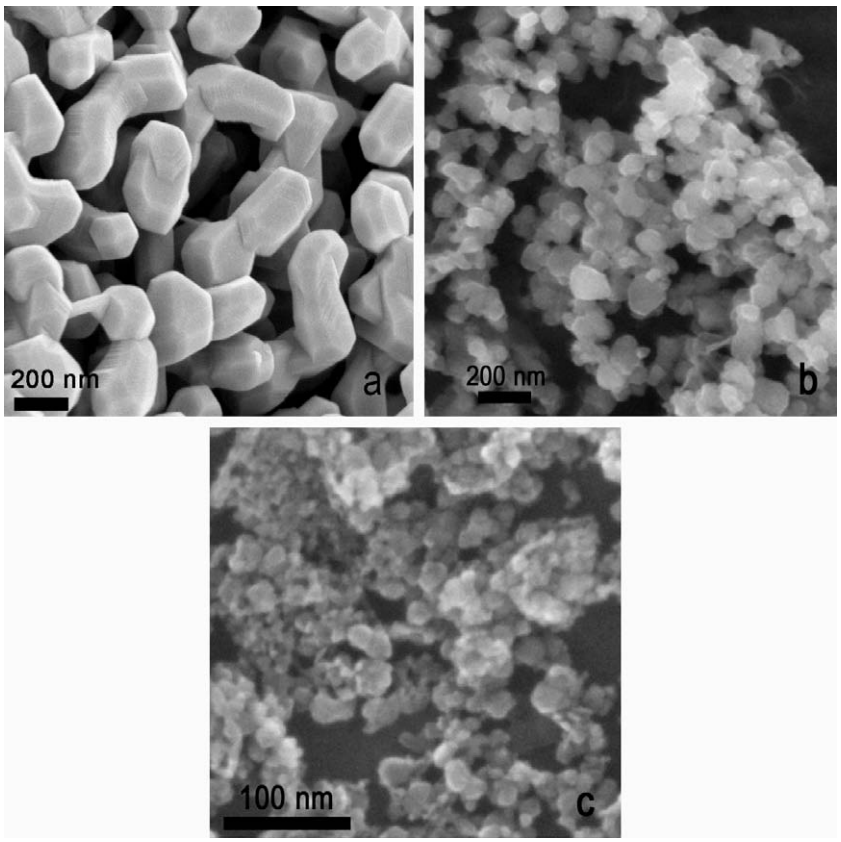

Fig. 1. SEM micrographs of magnetite (a), cobalt ferrite (b) and nickel ferrite (c).

(0.01 mol kg^{-1}) solutions were used as high temperature pH standards.

As can be shown from the surface complexation theory, the solid plays the role of a buffer and pH reaches the PZC for the highest concentration of the suspension [7,8]. However, the concentration for which the PZC is achieved depends on the starting pH. If the starting pH is close to the PZC, the latter can be reached for relatively small concentrations of suspension. This is illustrated in Fig. 2, taking the example of cobalt ferrite. The curves starting at pH 3 and 10.5 do not achieve a constant value of pH in the concentration range used, but indicate that the PZC is between 5 and 7. If we start at a pH close to 6, which is here the natural pH value without adding acid or base, a constant value is already achieved for a solid particle concentration of 50 g kg^{-1}.

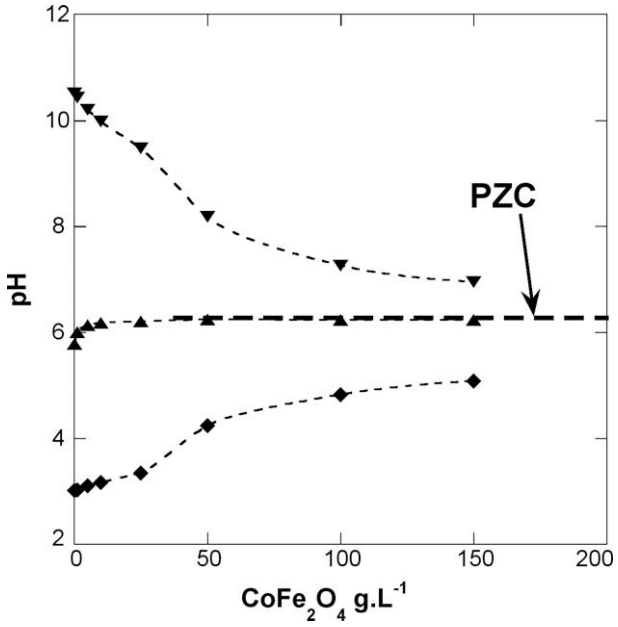

Fig. 2. Mass titration of cobalt ferrite at 25 °C in mol kg^{-1} KCl. Variation of pH with the concentration of solid particles in the suspension.

This method was used to determine the temperature dependency of PZC, without having to perform measurements with too many suspensions. After thorough experiments at 25 °C, concentrations close to 50 g kg^{-1} were used with an appropriate starting pH value at other temperatures. Between 5 and 50 °C, the measurements were performed in a thermostated bath. Between 50 and 320 °C measurements were performed in an autoclave.

2.3. Zetametry

Electrokinetic measurements were performed between 5 and 70 °C with a zetameter Malvern Zetasizer Nano ZS HT coupled to an automatic titrator. The pH was adjusted by addition of hydrochloric acid or potassium hydroxide. Preparation of suspensions and measurements were performed under nitrogen to avoid the effect of carbon dioxide. The ζ potential was calculated using the Henry and Oshima formula [4,14,15].

3. Results

3.1. Temperature dependency of PZC by mass titration

The PZC of magnetite and cobalt ferrite (Fig. 3 and Table 2) decreases with temperature until a minimum is observed. Then the PZC increases with increasing temperature. For comparison, values of the ionization constant of water K_w have been calculated

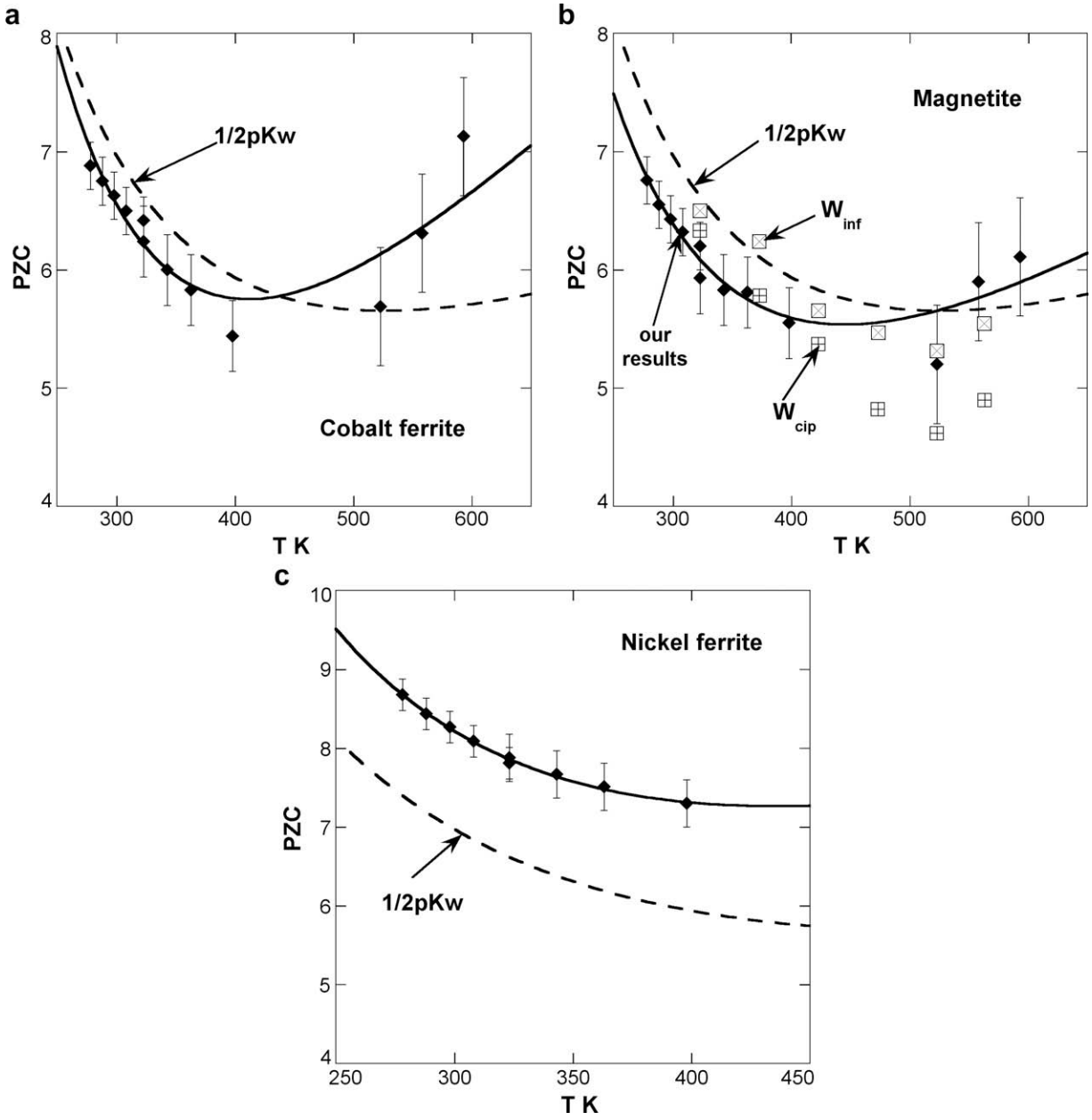

Fig. 3. Point of zero charge (PZC) obtained by mass titration for magnetite, cobalt ferrite and nickel ferrite versus temperature, including the fit of the PZC values represented by Eq. (8). Published experimental values of the magnetite PZC reported by Wesolowski et al. [27] are also shown where PZC_{infl} stands for PZC from the inflexion point of the titration curves and PZC_{cip} stands for PZC from the common intersection point. The variation of the pH of neutrality of water ($1/2pK_w$) is also shown.

according to *The International Association for the Properties of Water and Steam* recommendations [16] and the ½ pK_w curve versus temperature was drawn on Fig. 3. The behaviors are similar, but since the minimums are not situated at the same temperature, the PZC curves are seen to cross the ½ pK_w curve. Hence, the PZC of these particles is below the pH of neutrality of water below 250 °C for magnetite and below 150 °C for cobalt ferrite. At higher temperatures, the PZC is in the basic pH range of water.

In the case of nickel ferrite, the PZC was measured up to 125 °C. In the studied temperature range, the PZC is much higher than the pH of neutral point of water (Fig. 3).

3.2. Zetametry

The variation of ζ potential with pH for the three solids at 25 °C is shown on Fig. 4 for three different KCl concentrations. The ionic

Table 2
Values of the PZC obtained by mass titration for magnetite, cobalt ferrite and nickel ferrite in 10^{-2} mol kg^{-1} KCl 10^{-2} at different temperatures

T (°C)	PZC			
	Magnetite	Cobalt ferrite	Nickel ferrite	1/2 pK_w
5	6.6 ± 0.2	6.9 ± 0.2	8.9 ± 0.2	7.36
15	6.3 ± 0.2	6.7 ± 0.2	8.6 ± 0.2	7.17
25	6.2 ± 0.2	6.6 ± 0.2	8.5 ± 0.2	7.00
35	6.1 ± 0.2	6.5 ± 0.2	8.3 ± 0.2	6.84
50	6.0 ± 0.2	6.4 ± 0.2	8.0 ± 0.2	6.64
50	5.6 ± 0.3	6.2 ± 0.3	8.2 ± 0.3	6.64
70	5.5 ± 0.3	6.0 ± 0.3	8.0 ± 0.3	6.41
90	5.5 ± 0.3	5.8 ± 0.3	7.8 ± 0.3	6.21
125	5.2 ± 0.3	5.4 ± 0.3	7.6 ± 0.3	5.95
250	5.2 ± 0.5	5.7 ± 0.5	–	5.59
285	5.9 ± 0.5	6.3 ± 0.5	–	5.65
320	6.1 ± 0.5	7.1 ± 0.5	–	5.81

Values of the pH of neutrality of water (1/2 pK_w).

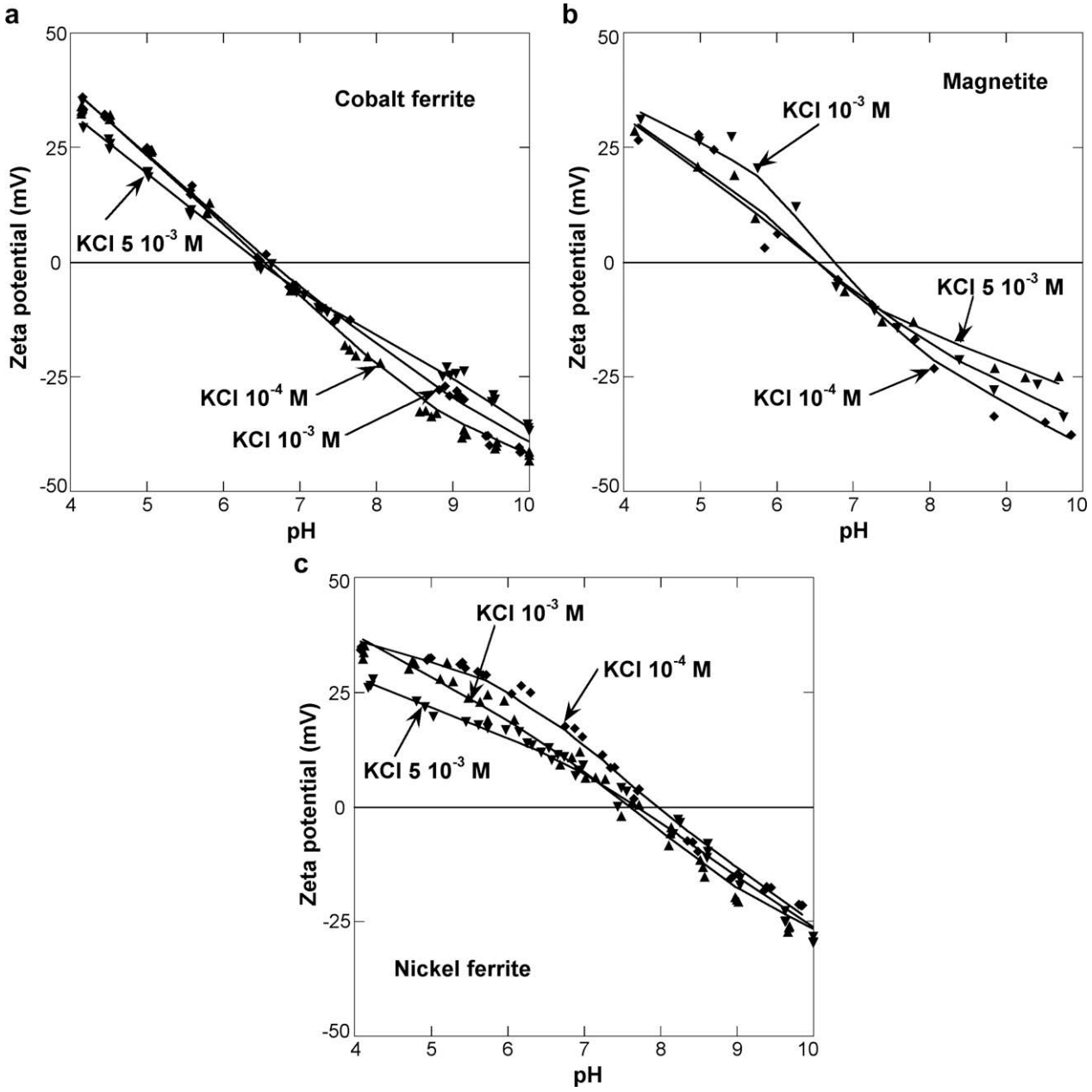

Fig. 4. Zeta potential of magnetite, cobalt ferrite and nickel ferrite at 25 °C versus pH for three different concentrations of potassium chloride (10^{-4}, 10^{-3} and 5×10^{-3} mol kg^{-1}).

strength did not have a significant influence in this KCl concentration range. The isoelectric point (IEP) is 6.6 ± 0.3 for magnetite, 6.5 ± 0.3 for cobalt ferrite and 7.7 ± 0.3 for nickel ferrite. The IEP of magnetite [17–19] and cobalt ferrite is close to previous reported values at 25 °C [20,21]. On the other hand, IEP of nickel ferrite is higher than the values reported earlier [22,23]. The difference in the behavior of nickel ferrite will be discussed later.

For magnetite and cobalt ferrite, the IEP at 25 °C is close to the PZC obtained by mass titration. This result validates the PZC measurements by mass titration. For nickel ferrite the difference between PZC and IEP is higher.

The influence of temperature was studied by measurements at 5 and 70 °C with a KCl concentration of 10^{-4} mol kg^{-1}. In the case of cobalt ferrite (Fig. 5), the IEP decreases as temperature increases. The IEP values are in good agreement with PZC measurements by means of mass titration. By contrast, the IEP of nickel ferrite seems to slightly increase with temperature (figure not given). The ζ potentials of magnetite could not be measured at 5 and 70 °C, due to rather fast agglomeration of particles and settlement.

4. Discussion

As already noted, nickel ferrite has different behavior from the two other solids in all types of measurements. We have compared the solubility and stability of the three solids as a function of pH and temperature by calculating the fractions of all dissolved and solid species with the computer code CHESS [24,25]. At low pH, the solids are totally transformed into hematite (Fe_2O_3) as solid phase and to Co^{2+}, Ni^{2+} or Fe^{2+} in solution. The pH range where this transformation occurs depends on the solid. Fig. 6 reports the fraction of the three studied solids remaining in the suspension versus pH. When temperature increases, the transition is shifted to lower pH and the nickel ferrite phase known as trevorite is transformed into bunsenite (NiO) [24,25].

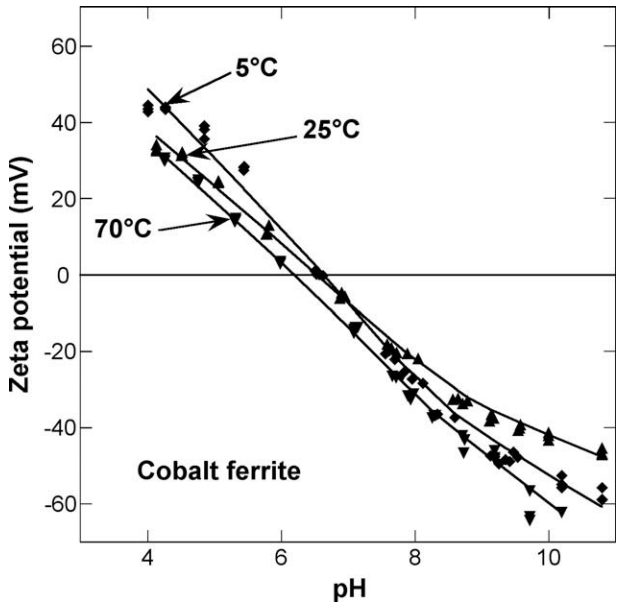

Fig. 5. Temperature effect on zeta potential of cobalt ferrite versus pH with a KCl concentration of 10^{-4} mol kg^{-1}.

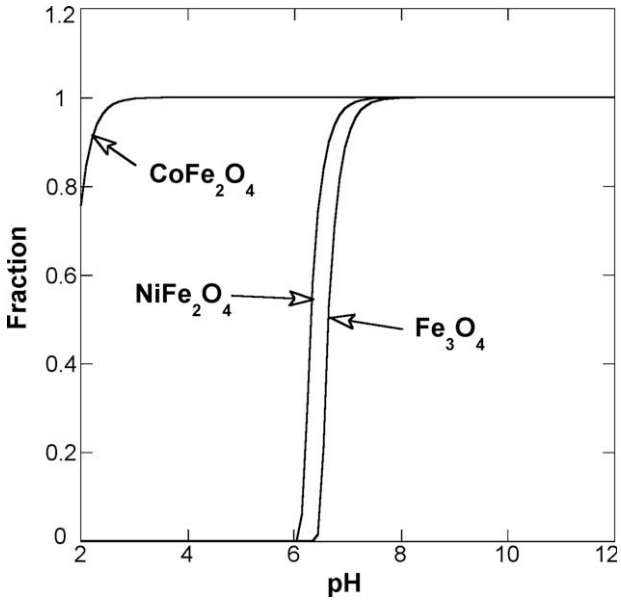

Fig. 6. Comparison of the stability and solubility of solids. The fraction of cobalt ferrite ($CoFe_2O_4$), nickel ferrite (trevorite, $NiFe_2O_4$) and magnetite (Fe_3O_4) is represented versus pH according to a simulation with code CHESS [24,25] at 25 °C.

Hence, the domain of stability of cobalt ferrite is larger than those of nickel ferrite and magnetite, which are thermodynamically unstable in a rather large part of experimental conditions studied. However, kinetics can considerably slow down these transformations and, in the case of magnetite, they seem not to have any effect on the surface charge.

The origin of the peculiar behavior of nickel ferrite may be its non stoichiometric composition with an excess of nickel, or its transformation into bunsenite.

4.1. Thermodynamic calculation

The aim of the following calculations is to model the temperature dependence of the PZC of magnetite, cobalt ferrite and nickel ferrite, in order to determine the thermodynamic constants and PZC for all temperatures in the studied range.

If we assume a 1-p*K* acid–base model [26], the protonation constant is defined as

$$\mathrm{M-OH_s^{-1/2}} + \mathrm{H_s^+} \rightleftarrows \mathrm{M-OH_{2s}^{+1/2}}$$

$$\mathrm{K} = \frac{[\mathrm{M-OH_{2s}^{+}1/2}]}{[\mathrm{M-OH_s^{-1/2}}][\mathrm{H^+}]_{\mathrm{Solution}}} \exp\left(\frac{e\Psi_0}{kT}\right), \tag{1}$$

where $[M-OH_{2s}^{+1/2}]$ and $[M-OH_s^{-1/2}]$ are the concentrations of the charged surface groups resulting from protonation and deprotonation, respectively, $[H^+]_{Solution}$ the hydrogen ion concentration in the bulk solution, K the protonation constant, Ψ_0 the surface potential, e the electronic charge, k the Boltzmann's constant, T the Kelvin temperature.

At the PZC, $[M-OH_{2s}^{+1/2}]$ equals $[M-O_s^{-1/2}]$ and Ψ_0 equals zero. Formula (1) simplifies to

$$\log K = \mathrm{PZC}, \tag{2}$$

where PZC is the pH in the bulk solution at the point of zero charge. Neglecting the impact of pressure, the variation of the free enthalpy $\Delta_r G$ *is*

$$\Delta_r G = \Delta_r G^0 + RT\ln K, \tag{3}$$

where $\Delta_r G^0$ is the variation of the standard free enthalpy and R the gas constant. When the equilibrium is reached, $\Delta_r G = 0$ and Eq. (3) becomes:

$$\Delta_r G^0 = -RT\ln K = \Delta_r H^0 - T\Delta_r S^0, \tag{4}$$

where $\Delta_r H^0$ is the standard enthalpy and $\Delta_r S^0$ the standard entropy of single protonation. By combining Eqs. (2) and (4), the PZC can be expressed as

$$\mathrm{PZC} = \frac{1}{R\ln(10)}\left(-\frac{\Delta_r H^0}{T} + \Delta_r S^0\right). \tag{5}$$

If we assume that $\Delta_r C_p^0$, the variation of the heat capacity, is constant over the studied temperature interval:

$$\begin{aligned}\Delta_r H^0(T) &= \Delta_r H^0(T_0) + \int_{T_0}^{T} \Delta_r C_p^0(T_0)\mathrm{d}T \\ &= \Delta_r H^0(T_0) + \Delta_r C_p^0(T_0)(T - T_0),\end{aligned} \tag{6}$$

and:

$$\begin{aligned}\Delta_r S^0(T) &= \Delta_r S^0(T_0) + \int_{T_0}^{T} \frac{\Delta_r C_p^0(T_0)}{T}\mathrm{d}T \\ &= \Delta_r S^0(T_0) + \Delta_r C_p^0(T_0)\ln\frac{T}{T_0}.\end{aligned} \tag{7}$$

The relation of PZC with the thermodynamic constants of single protonation for a temperature T *is*

$$\begin{aligned}\mathrm{PZC}(T) = &\frac{1}{R\ln(10)} \\ &\times\left[-\frac{\Delta_r H_{298}^0 + \Delta_r C_p^0(298 - T)}{T} + \Delta_r S_{298}^0 + \Delta_r C_p^0\ln\left(\frac{T}{298}\right)\right].\end{aligned} \tag{8}$$

If we had considered a 2-p*K* model, we could, in the same manner, connect the PZC to the thermodynamic parameters of the double protonation.

The thermodynamic constants were obtained by fitting the experimental values of PZC versus temperature by Eq. (8), using a least squares method weighted by experimental errors. Results are reported in Table 3 and Fig. 3. Error bars, connected to the

Table 3
Thermodynamic parameters of the single protonation of magnetite, cobalt ferrite and magnetite at 298 K

	$\Delta_r H^0_{298}$ (kJ mol^{-1})	$\Delta_r S^0_{298}$ (J K^{-1} mol^{-1})	$\Delta_r C^0_p$ (J K^{-1} mol^{-1})
Magnetite	−27 ± 5	32 ± 20	183 ± 70
Magnetite[a]	−29 ± 5	25.5[b]	204 ± 33
Cobalt ferrite	−31 ± 5	20 ± 19	276 ± 71
Nickel ferrite	−32 ± 7	52 ± 29	227 ± 26

$\Delta_r H^0_{298}$: standard enthalpy, $\Delta_r S^0_{298}$: standard entropy and $\Delta_r C^0_p$: heat capacity variation.

[a] Resulting of best-fit parameters for magnetite obtained from inflection points of titration curves by Wesolowski et al. [27].

[b] Value of ΔS^0_{298} fixed by Wesolowski et al. [27] to better constrain the fit.

uncertainty on pH values, are relatively large at high temperature. Their values have an impact on the errors on thermodynamic constants. However, the increase of the PZC over 400 K is well established for cobalt ferrite and magnetite.

The value of $\Delta_r H^0_{298}$ for magnetite is in good agreement with the value (−32.4 kJ mol^{-1}) obtained by Wesolowski et al. [27] between 50 and 290 °C from the inflexion points of titration curves. The PZC values obtained by the same authors from the common intersection point (CIP) are in lesser agreement with our values. According to the review made by Kosmulski [28], the variation of the standard enthalpy of single protonation at 298 K of oxides ranges between 0 to −80 kJ mol^{-1} with a majority of measurements between −10 and −40 kJ mol^{-1}. As a comparison, the calculated standard enthalpy of protonation of water is −30 kJ mol^{-1} [16].

The high error interval on $\Delta_r S^0_{298}$ is explained by the small influence of entropy in formula (8). In their calculations, Wesolowski et al. [27] imposed a fixed value for $\Delta_r S^0_{298}$ of 25.5 J K mol^{-1}. In Table 3, we have also reported a calculation of the enthalpy of protonation of magnetite with this imposed value of entropy.

As already noted, the difference $|1/2\ pK_w - PZC|$ is not constant all over the studied temperature range and the PZC curves cross the ½ pK_w curve. Hence, the PZC of these particles is below the pH of neutrality of water below 250 °C for magnetite and below 150 °C for cobalt ferrite. At higher temperatures, the PZC is in the basic pH range of water. The greater affinity of magnetite and cobalt ferrite towards hydrogen ions at high temperature compared to the affinity of water, would increase the bulk solution pH.

In the case of nickel ferrite (Fig. 3 and Table 2), the PZC decreases as the temperature increases in the temperature range studied (5–125 °C). Its values are higher than ½ pK_w, but almost parallel to its variation.

During operation, the temperature of the PWR's primary circuit fluid ranges from 285 °C (far from the reactor core) to 320 °C (in the core) and its pH, at these temperatures, is close to 7 and slightly higher. This pH is about one pH unit higher than the point of zero charge of magnetite, indicating that the charge of these particles should be negative. In the case of cobalt ferrite, the pH of the fluid is closer to the PZC, so that particles should be neutral or slightly negative. For nickel ferrite, if $|1/2\ pK_w - PZC|$, remains constant above 125 °C, its PZC could be close to pH 7 between 285 and 320 °C. As a result, in these conditions, electrostatic interactions could be of small influence for ferrites, which is in favor of adhesion, since, in this case, attractive Van der Waals forces will be dominating. For magnetite, whose surface is negative, adhesion would depend on the charge of the materials constituting the walls of the primary circuit. According to Guillodo et al. [29], the surface of a 690 alloy is positive in the conditions of the primary circuit, so magnetite, whose surface has an opposite charge, should adhere to this alloy. For ferrites, whose surfaces are neutral or slightly negative, adhesion is also favored.

It should be noticed, that another important factor, not studied here and which could modify the surface charge and the adhesion behavior, is the sorption of dissolved species. Borate ions are certainly a species which could have the main influence. A better knowledge of the PZC of all materials (690 alloy, zircaloy,...) in contact with the fluid is also necessary, to have a more accurate prediction of the adhesion.

5. Conclusion

Knowledge of the temperature dependence of PZC of metal and metal oxides found in PWRs is important for the development of models that can help to better understand the importance of colloids in the contamination of the primary circuit. For the first time, to our knowledge, the variation of the point of zero charge of three typical oxides found as colloids in PWR primary circuits has been measured between 5 and 320 °C and their protonation thermodynamic constants calculated. The sign of their surface charge and their adhesion behavior can be thus predicted in this temperature range. Results show that, in the operating temperature of PWR, adhesion of magnetite, cobalt ferrite and nickel ferrite particles is favored. Investigations are in progress in order to complete these basic results on acid–base properties of oxide particles by experiments in presence of species (borate, lithium ions) found in primary circuits of PWR. Other studies are devoted to an accurate measurement of the PZC of materials constituting the walls of the PWR primary circuits. These results will lead to a more accurate prediction of the adhesion of colloidal species in PWR, with the aim to improve procedures used to remove 'hot' spots and, in the future, minimize deposition.

References

[1] G.C.W. Comley, Prog. Nucl. Energy 16 (1985) 41.
[2] F.A. Means, R.S. Rodliffe, K. Harding, Nucl. Technol. 47 (1980) 385.
[3] A. Rocher, P. Ridoux, S. Anthony, C. Brun, Program to eradicate hot spots (Co-60) carried out in French PWR units, in: International Conference on Water Chemistry in Nuclear Power Plants, Kashiwasaki, Japan, 13–16 October 1998, p. 161.
[4] R.J. Hunter, Foundations of Colloid Science, Oxford University Press, New York, 2001.
[5] G. Lefèvre, A. Hamza, M. Fédoroff, F. Carette, H. Cordier, Colloids Surf. A 280 (2006) 32.
[6] J. Westall, H. Hohl, Adv. Colloid Inter. Sci. 12 (1980) 265.
[7] P.H. Tewari, A.B. Campbell, J. Colloid Interf. Sci. 55 (1976) 531.
[8] J.S. Noh, J.A. Schwarz, J. Colloid Interf. Sci. 130 (1989) 157.
[9] Y. Solomon, J. Roesmer, Nucl. Technol. 29 (1976) 166.
[10] Y.L. Sandler, Corros. Nace 35 (1979) 205.
[11] L.W. Niedrach, J. Electrochem. Soc. 127 (1980) 2122.
[12] D.D. Macdonald, S. Hettiarchchi, S.J. Lenhart, J. Solution Chem. 17 (1988) 719.
[13] D.D. Macdonald, S. Hettiarachchi, H. Song, K. Makela, R. Emerson, M. Ben-Haim, J. Solution Chem. 21 (1992) 849.
[14] D.C. Henry, Proc. Roy. Soc. Lond. A 133 (1931) 106.
[15] H. Oshima, J. Colloid Interf. Sci. 168 (1994) 269.
[16] The International Association for the Properties of Water and Steam, Guideline on the Use of Fundamental Constants and Basic Constants of Water, Gaithersburg, Maryland, USA, 9–4 September 2001.
[17] M.A. Blesa, A.J.G. Maroto, A.E. Regazzoni, J. Colloid Interf. Sci. 99 (1984) 32.
[18] R.C. Palza, J.L. Arias, M. Espin, M.L. Jiménez, A.V. Delgado, J. Colloid Interf. Sci. 245 (2002) 86.
[19] O. Perales Perez, Y. Umetsu, H. Sasaki, Shigen-to-Sozai 116 (2000) 297.
[20] J. de Vincente, A.V. Delgado, R.C. Plaza, J.D.G. Duran, F. Gonzalez-Caballero, Langmuir 16 (2000) 7954.
[21] J. de Vincente, J.D.G. Duran, A.V. Delgado, Colloids Surf. A 195 (2001) 181.
[22] R.C. Plaza, J. de Vincente, S. Gomez-Lopera, A.V. Delgado, J. Colloid Interf. Sci. 242 (2001) 306.
[23] A.E. Regazzoni, E. Matijevic, Corros. NACE 38 (1982) 212.
[24] J. Van der Lee, Jchess 2.0, Ecole des mines de Paris, Centre d'Informatique Géologique, 2000–2001, <http://www.chess.ensmp.fr>.
[25] Jchess 2.0 data base, The Thermodynamic Research Laboratory of the University of Illinois at Chicago.
[26] G.H. Bolt, W.H. Van Riemsdijk, G.H. Bolt (Eds.), Soil Chemistry, B: Physico-chemical Models, Elsevier, Amsterdam, 1982 (Chapter 13).
[27] D.J. Wesolowski, M.L. Machesky, D.A. Palmer, L.M. Anovitz, Chem. Geol. 167 (2000) 193.
[28] M. Kosmulski, Chemical Properties of Material Surfaces, 102, Marcel Dekker, New York, Basel, 2001.
[29] M. Guillodo, P. Combrade, B. dos Santos, T. Muller, G. Berthollon, N. Engler, C. Brun, G. Turluer, in: International Conference on Water Chemistry of Nuclear Reactor Systems, San Francisco, USA, 11–14 October 2004.